Chem Soc Rev

REVIEW ARTICLE

View Article Online
View Journal | View Issue

Cite this: *Chem. Soc. Rev.*, 2015, 44, 6519

Recent developments and future prospects of all-metal aromatic compounds

Jose M. Mercero,[a] Alexander I. Boldyrev,[b] Gabriel Merino[c] and Jesus M. Ugalde*[d]

Received 24th April 2015

DOI: 10.1039/c5cs00341e

www.rsc.org/chemsocrev

The usefulness of aromaticity/antiaromaticity concepts to foresee structural stability patterns and salient features of the electronic structure of small inorganic and all-metal rings has been put forward. A critical revision of the advances made in the theoretical methods to assess the aromaticity/antiaromaticity of these compounds has also been made. In particular, the performance of local *versus* non-local indices has been reviewed. Finally, the passivation of these rings has been put forward as a key issue in order to prevent them from collapsing into larger aggregates and to provide them protection against the environment.

1 Introduction

Aromaticity in chemistry was introduced by German chemist Friedrich August Kekulé,[1,2] who used this term to characterize unexpectedly low reactivity in a set of molecules, derivatives of benzene. Molecules in his aromatic set actually had a specific odour. Since that, the aromaticity "*tent*" has been extended to a large number of organic species starting from the $C_3H_3^+$ cyclopropenyl cation[3] to polycyclic hydrocarbons,[4] which are present in oil, coal and even in DNA molecules and all building-blocks that support all known forms of life. Today we think that aromaticity exists because of a specific chemical bonding pattern, which cannot be represented by a single Lewis structure, and consequently, we need to use either a resonance of few Lewis structures or a multicenter bonding type description in order to get a chemical bonding structure consistent with the usually high symmetry geometry of aromatic molecules.

Aromaticity itself constitutes one of the many useful but loosely defined concepts that conform modern chemistry concepts' toolbox. Some of them, aromaticity included, have no precise meaning and do not denote directly measurable

[a] *IZO-SGI SGiker, Euskal Herriko Unibertsitatea (UPV/EHU), P.K. 1072, 20080 Donostia, Euskadi, Spain*
[b] *Department of Chemistry and Biochemistry, Utah State University, 0300 Old Main Hill, Logan, UT 84322, USA*
[c] *Departamento de Física Aplicada, Centro de Investigación de Estudios Avanzados, Unidad Mérida, Km. 6 Antigua Carretera a Progreso, A.P. 73, Cordemex, Mérida 97310, Mexico*
[d] *Kimika Fakultatea, Euskal Herriko Unibertsitatea (UPV/EHU) and Donostia International Physics Center (DIPC), P.K. 1072, 20080 Donostia, Euskadi, Spain*

Jose M. Mercero

Jose M. Mercero graduated in 1995 at UPV/EHU after having spent one year as an exchange student at Universiteit Utrecht and another at the University of North Carolina at the Chapell Hill. He completed his PhD (with honors) in 2001 under the supervision of Prof. Jesus M. Ugalde at UPV/EHU. Afterwards, he held a Postdoctoral position in Prof. Ugalde's group from 2001 to 2004. Since then, he is in charge of the Scientific Computing Department of the IZO-SGI SGIker at the UPV/EHU.

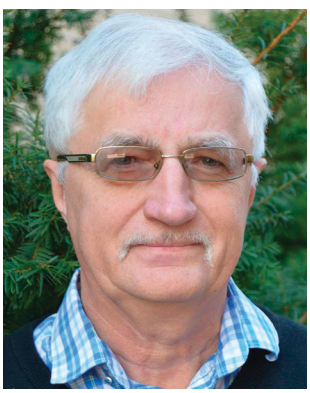

Alexander I. Boldyrev

Alexander I. Boldyrev was born in Siberia, Russia (1951), and received his BS/MS (1974) in chemistry from Novosibirsk University, his PhD in physical chemistry from Moscow State University, and his Dr Sci. in chemical physics from Moscow Physico-Chemical Institute (1984). He is currently a professor in the Department of Chemistry and Biochemistry at Utah State University. His current scientific interest is the development of chemical bonding models capable of predicting the structure, stability, chemical bonding, and other molecular properties of pure and mixed clusters, low-dimensional materials and solids.

quantities, albeit they are based mostly on experimentally "observable" measurements. Thus, aside from their "aroma", not necessarily always nice, it is firmly established that "aromatic" molecules are often more stable and their geometries more regular than expected *a priori*. Additionally, they are barely reactive, in spite of having a number of unsaturated bonds. These unsaturated bonds are not localized, but delocalized through the molecule and confined within the molecule.

Hückel in 1931 formulated his $(4n + 2)$ rule[5–8] for the ground singlet states of ring-like molecules having delocalized π-type molecular orbitals, n being the number of delocalized π-type molecular valence electrons. Hückel's formula establishes the link between the molecular electronic structure and aromaticity, which was completed by Baird who found that for spin states of multiplicity higher than singlet Hückel's electron counting rule should be modified accordingly.[9] Further extensions of Baird's rule have been revised recently.[10–13] Thus, in the beginning it was thought, in accordance with Hückel's theory, that aromatic molecules were annular like with $(4n + 2)$ atomic p-type electrons arranged in spin-coupled pairs into $(2n + 1)$ π-type delocalized molecular orbitals, n being an integer number, *i.e.:* $n \in \mathcal{N}$. However, these constrains were soon lifted and thus, Dewar[14,15] introduced the concept of σ-aromaticity to account for the anomalous magnetic behavior of cyclopropane by extending Hückel's aromaticity rule to the skeletal σ-type electrons. Although explicit evaluation of the σ-aromatic stabilization energy of cyclopropane relative to propane[16] amounts only 3.5 kcal mol^{-1} and, hence, fails to provide strong evidence for any σ-aromatic effect, the concept has found its way ahead as a key feature for explaining the magnetic and energetic properties of a series of inorganic ring-like clusters.[17] These two types of aromaticities (π-type and σ-type) have been found to occur simultaneously in many molecules.[18] Sometimes they *cooperate* to render an enhancement of the aromaticity and sometimes they act antagonistically lowering the aromaticity. Finally, Breslow introduced in chemistry a concept of anti-aromaticity.[19] Unlike aromatic molecules, antiaromatic compounds are highly unstable and highly reactive and they obey the Hückel $(4n)$ either σ or π rule.

Nonetheless, Hückel's $(4n + 2)$ and $(4n)$ rules for aromaticity and antiaromaticity, respectively, provide simple probes of aromaticity and antiaromaticity from the molecular electronic structure perspective. These probes are only qualitative, "*yes or no*" like. They tell us whether a molecule is (anti)aromatic or not, but do not tell us how much (anti)aromatic it is. In order to get a quantitative approach to (anti)aromaticity, we need to use other probes,[20] such as the energetic criterion, the geometric criterion, the magnetic criterion, and probes for the reactivity of the particular chemical system.[21]

Aromaticity and antiaromaticity have also been extended to the realm of non-carbon molecules. All-metal aromatic compounds[22] have attracted increased interest since the earlier prediction of the aromaticity of transition metal metallocyclopentadienyls, made by Thorn and Hoffmann[23] in 1979. Recently, Bleeke,[24,25] Wright,[26] Lanford and Haley,[27] and Fernández *et al.*[28] have reviewed the significant progress made in the chemistry of transition metal metallocycles.

Aside from metallocycles, which contain binary rings made of metals and carbon, organometallic coordination compounds containing *all-metal* aromatic rings have also been synthesized. The earlier ones belong to a family of group 13 three-membered rings and were investigated by Robinson *et al.*[29–32] Dipotassium tris((2,6-dimesitylphenyl)cyclogallene), $K_2[Ga_3R_3]$, with R = $(Mes_2C_6H_3)$ and (Mes = 2,4,6-$Me_3C_6H_2$), was the first one synthesized (see Fig. 1). This molecule posses a stabilizing doubly occupied π-type valence molecular orbital delocalized over the three gallium atoms,[29] which satisfies the Hückel aromaticity electron counting rule $(4n + 2)$ with $n = 0$.

Gabriel Merino

Gabriel Merino was born in Puebla (México) in 1975. He received his PhD from Cinvestav in 2003 under the supervision of Prof. Alberto Vela. After a two-year period as Postdoctoral Associate at Technische Universitt Dresden (Prof. Gotthard Seifert and Prof. Thomas Heine), Gabriel started his independent career at Universidad de Guanajuato. In 2012, he joined the Department of Applied Physics at Cinvestav Mérida. His group is focused on predicting molecular systems that violate what is established by traditional chemistry and that allow taking to the limit basic concepts like structure, chemical bond, and aromaticity. He has co-authored 110 articles and was awarded the 2012 Academia Mexicana de Ciencias and the Moshinsky Foundation Awards.

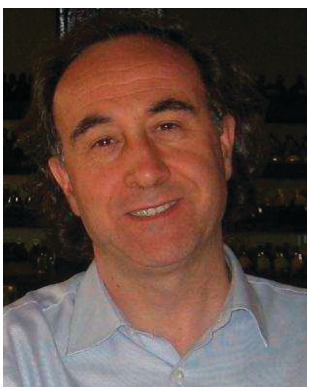

Jesus M. Ugalde

Jesus M. Ugalde, born in 1957 in Bergara, the Basque town where Tungsten was isolated in 1783, graduated in 1981, and got his PhD from the University of Valladolid in 1984. He made postdoctoral stays at ORNL, with Rufus Ritchie, and Cornell University with Roald Hoffmann. For many years he collaborated closely with Prof. Russell J. Boyd, Dalhousie University, until he got his position as Professor of Chemistry at the University of the Basque Country in 1994. He is currently the president of the Basque Academy of Sciences, Arts and Letters.

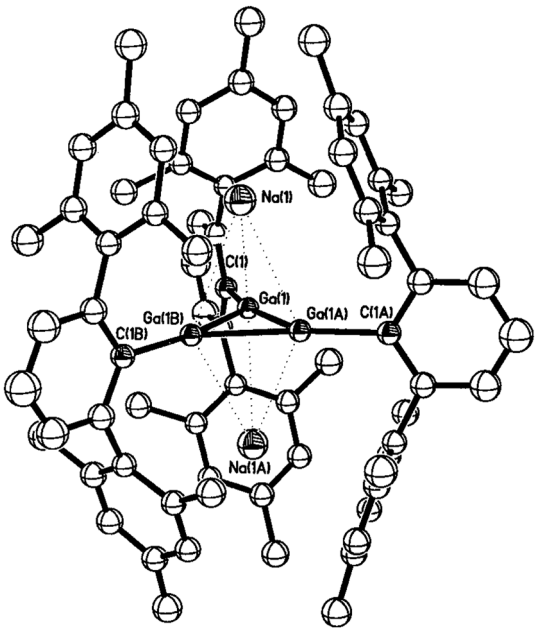

Fig. 1 Crystal structure of $Na_2[Ga_3R_3]$, R = ($Mes_2C_6H_3$). Reproduced with permission from ref. 31. Copyright 1999, American Chemical Society.

Subsequent theoretical analysis of the $M_2[Ga_3H_3]$, M = Li, Na and K, model compounds[33] revealed that the $Ga_3H_3^{2-}$ core is indeed best described as *metalloaromatic*, which contains a metal ring system exhibiting traditional (organic) aromaticity. This has permitted us to take a new look to a number of inorganic salts, already reported in the open inorganic chemistry literature. Thus, compounds, such as $(2,2,2\text{-crypt-}K^+)_2Sb_4^{2-}$ salt containing planar square Sb_4^{2-},[34] $[(\eta^5\text{-}1,2,3\text{-}t\text{Bu}_3C_5H_2)Mo(\mu,\eta^5\text{-}Sb_5)\text{-}Mo(\eta^5\text{-}1,2,3\text{-}t\text{Bu}_3C_5H_2)]$ and $[(\eta^5\text{-}1,2,4\text{-}t\text{Bu}_3C_5H_2)Mo(\mu,\eta^5\text{-}Sb_5)\text{-}Mo(\eta^5\text{-}1,4\text{-}t\text{Bu}_2\text{-}2\text{-MeC}_5H_2)]$ containing a slightly distorted antimony pentagon Sb_5^- ring,[35] and 2,2,2-crypt-potassium tetrabismuthide^{2-}, a $(C_{18}H_{36}N_2O_6K^+)_2Bi_4^{2-}$ compound containing a perfectly planar square Bi_4^{2-} dianon,[36] can be described with the help of aromaticity.

Since then, the structure of a number of additional metalloids and metal rings has been revised and their geometrical and electronic structural features were rationalized in terms of aromaticity. Thus, the experimental characterization of the planar square rings Se_4^{2+} and Te_4^{2+} dications has been communicated,[37–39] as well as the Sb_7^- anion.[40] In the same vein, the planar pentagonal rings, As_5^-, Sn_5^{6-} and Pb_5^{6-} which have been experimentally characterized[41–43] and Si_5^{6-},[44] can be best described as all-metal aromatic rings. Also, ring-like compounds of transition metal elements only have been reported to show signs of δ-aromaticity, as arising from the full occupation of the bonding molecular orbitals made of the linear combinations of their d_{z^2}-type atomic orbitals.[45–47] Since the introduction of aromaticity to metal systems, many new aromatic/antiaromatic chemical species composed of main groups and transition metal atoms were discovered. These new advances have been recently reviewed.[22,47–57]

Finally, it is worth mentioning that aromaticity has also been extended to three dimensional systems and the term *spherical* aromaticity coined[58,59] for polyhedral hollow molecular structures with $2(n+1)^2$, $n \in \mathcal{N}$, delocalized electrons. However, in this review we shall be concerned with aromaticity in planar *n*-membered all-metal ring-like compounds.

2 The advantages of planarity: the aromaticity of small boron clusters

Planarity is one of the most salient common features of aromatic organic molecules,[60] and this imposes stringent constraints to their electronic structure because they must conform to the symmetry and the boundary conditions set up by confining attractive potential of the actual molecular framework. Thus, the stability of the electronic structure of the delocalized electrons is found to be very sensitive to the number of delocalized electrons within the molecular framework and to the geometrical deformations of that structure relative to its high symmetry one. This well-known feature of carbon aromatic molecules can also be seen in molecules made of elements other than carbon. The B_{13}^+ cluster constitutes one such example where planarity provides a means of acquiring additional stabilization through aromaticity.

The B_{13}^+ bare cluster was first proved to be an intriguing species through the experiments carried out in Anderson's laboratory.[61] They noted that the mass distribution of their laser ablated boron rods yields numerous "magic numbers" in the range of n = 1–20. However, when these resulting clusters were proven by collision induced dissociation experiments, only B_5^+ and B_{13}^+ appeared to be especially stable, both showing significant differences in the appearance potentials for B^+ and B_{n-1}^+ when compared to clusters of similar size. Furthermore, for B_{13}^+ the appearance potential for B^+ was found to be lower than that for B_{12}^+, in sharp contrast to other clusters for which the appearance potential for B^+ is found to be always greater than that for B_{n-1}^+. Subsequent reactivity studies of boron clusters showed that B_{13}^+ was anomalously unreactive.

Anomalous experimental findings provide a favorite playground for theoreticians, and as such, the case of the B_{13}^+ cluster did not pass unnoticed. After Anderson's reports on the bizarre behavior of B_{13}^+ were published, a number of theoretical studies, aimed to elucidating the geometrical structure of its ground state, appeared. Kawai and Weare, Boustani, Ricca and Bauschlicher and Fowler and Ugalde contributed to this endeavor and, finally, it was established by Ricca and Bauschlicher[62] that the ground state structure of B_{13}^+ was the planar C_{2v} symmetry shown on the left of Fig. 2. It was, nonetheless, disturbing that the most stable isomer of B_{13}^+ was not a 3D filled icosahedral structure, for it was thought that its high stability could be attributed to the structural compactness provided by such a 3D structure with maximized atomic coordination. In this context, the planarity of B_{13}^+ was seen an impediment towards its lack of reactivity.

However, Fowler and Ugalde[63] noticed that B_{13}^+ could indeed take advantage of its planarity. They proposed that the unexpected stability of B_{13}^+ was ascribable to its aromatic

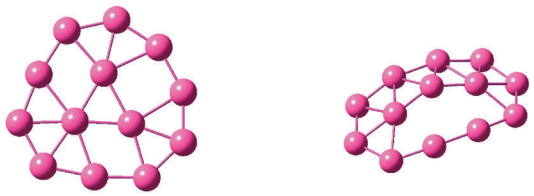

Fig. 2 B_{13}^+ most stable complexes. Ricca structure, at the left hand side is around 27 kcal mol^{-1} more stable than Boustani structure (right hand side).

character, an observation based on the calculated doubly occupied π-molecular orbitals of B_{13}^+, which were found to be reminiscent of those benzene and consequently of Hückel aromaticity.

Fig. 3 compares the Kohn–Sham π-orbitals of benzene (b) and the corresponding molecular orbitals of B_{13}^+ Ricca (r) and Boustani's (B)[64] structures. The orbital nodes are marked, and observe that orbitals with 0 and 1 nodes are binding orbitals while the 2 node orbitals are antibonding. On the other hand, the molecular orbitals of the Ricca isomer resemble, basically, π-molecular orbitals of a round system like benzene. Remembering basic Hückel molecular orbital theory of aromaticity, six electrons (that is: $4n + 2$, with $n = 1$) must fill three π-molecular orbitals, the lowest one in energy being nondegenerate with no nodes and the remaining two π-molecular orbitals being degenerate having one node each. This is exactly the case of the Ricca isomer as shown in Fig. 3. The MOs of the Boustani system are split because of their oval shape. Both the Boustani and Ricca cationic clusters have six π-electrons, meaning that the orbitals labeled 0, 1a, and 1b (where the numbers indicate the number of nodes) are filled with two electrons each. Note that the cationic Boustani structure adopts a C_s structure so that the central atom does not lie along the central node shown in 1a of Fig. 3. This reduces the favorable interactions between that atom and the two atoms on the other side of the loop. Considering this geometric feature and the highly favorable π-delocalization of the rounder Ricca structure helps in understanding why this structure is the most stable for the cations.

This simplified molecular orbital diagram accounts also for the stability of the neutral and anionic forms of the B_{13} cluster. As we move to the neutral and anionic cases, electrons are placed in the π-molecular orbitals with two nodes. The 2a orbital of the Boustani cluster will, of course, be filled first,

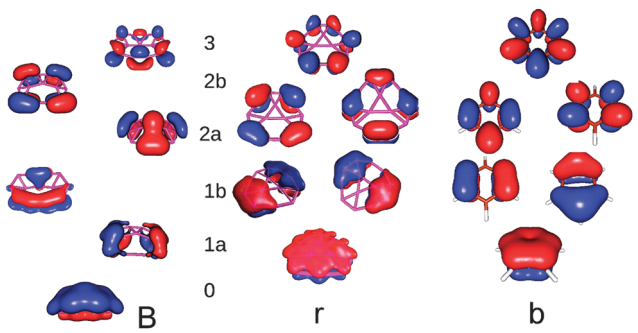

Fig. 3 The π-molecular orbitals of the Boustani (B) and Ricca (r) isomers of B_{13}^+ compared with those of benzene (b).

but the Ricca cluster has open a pair of quasi-degenerate orbitals, both of which lie higher in energy than that available for the Boustani isomer. Thus, the addition of one electron to the cationic clusters reduces the energetic difference between both of them. This effect is repeated when a second electron is added making the Boustani anion more stable than the Ricca anion. This very basic diagram is in perfect agreement with the prediction of a singlet ground state for the Boustani anion, a triplet ground state for the Ricca anion, and the difference in relative energies among the various charge states. It is also in support of the argument that the B_{13}^+ cationic cluster is especially stable because it is aromatic.

In support of this interpretation, Aihara evaluated the topological resonance energy (TRE) for the π-electrons of B_{13}^+ using graph theory.[65] He found that the TRE of Ricca's isomer of B_{13}^+ is positive in sign and very large in magnitude: TRE = $2.959|\beta_{BB}|$. This number can be compared to aromatic hydrocarbons with similar size, such as phenalenium ($C_{13}H_9^+$) TRE = $0.410|\beta_{BB}|$, anthracene ($C_{14}H_{10}$) TRE = $0.475|\beta_{BB}|$, and phenanthrene ($C_{14}H_{10}$) TRE = $0.576|\beta_{BB}|$. On the basis of the TRE value, B_{13}^+ is much more aromatic than polycyclic aromatic hydrocarbons of similar molecular sizes.

Finally, it is worth mentioning that like in the case of other large boron clusters, the σ-bonding was discussed later by Wang and Boldyrev.[66] According to their σ-bonding analysis, the B_{13}^+ cation is also a σ-aromatic system. Indeed, they showed that, out of the 19 MOs, 10 σ-MOs are responsible for 10 2c–2e B–B peripheral bonds, 3 σ-MOs are responsible for 3 2c–2e B–B bonds between central boron atoms, and 3 σ-MOs are responsible for global delocalized bonding between the 3 central boron atoms and the 10 peripheral boron atoms. Consequently, B_{13}^+ is best described as a doubly (σ- and π-) aromatic system.

This double aromaticity is responsible not only for its rather round shape, extra stability, and low reactivity, but also for a number of dynamical properties which could find applications in molecular devices' science.[67,68] Thus, Martínez-Guajardo *et al.*[69] demonstrated computationally that B_{13}^+ has a fluxional behavior featuring an almost free rotation of the inner B_3 moiety with respect to the outer B_{10} ring. The relative rotation of the concentric B_3 equilateral triangle and the B_{10} ring of B_{13}^+ was further examined by Zhang *et al.*,[70] who proposed that the relative rotation of the two moieties of B_{13}^+ could be triggered by applying an external laser field. When a circularly polarized external electric field is applied perpendicular to the molecule plane, the symmetry is broken and the system is expected to preferentially rotate unidirectionally because one of the directions is essentially barrierless while the other is hindered by a heightened energy barrier.

Wang and Boldyrev during their fifteen years joint experimental and theoretical quest for understanding the geometric and electronic structure of negative boron clusters established that small and medium size boron clusters are planar or quasi-planar and developed a comprehensive chemical bonding model based on double aromaticity, which is able to rationalize chemical bonding in these clusters.[66,71] They showed how this

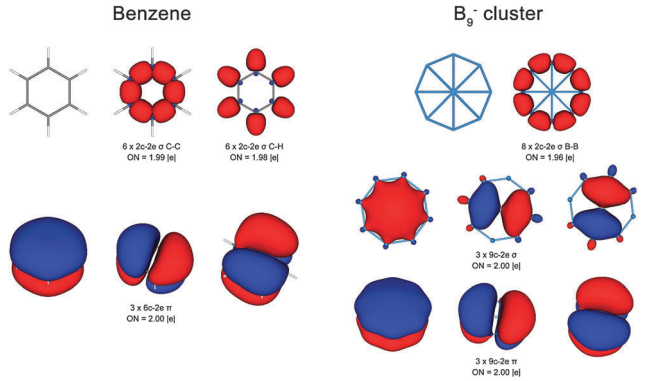

Fig. 4 Adaptive Natural Density Portioning chemical bonding pattern of the benzene molecule and the B_9^- cluster. ON stands for occupation numbers.

multiple aromaticity helps to understand why the B_9^- cluster has a beautiful wheel-like structure (Fig. 4). In Fig. 4 it is compared side-by-side the chemical bonding pattern obtained from the Adaptive Natural Density Partitioning (AdNDP) method[72] for the prototypical aromatic benzene molecule and the B_9^- cluster.[73]

The bonding in B_9^- is intractable using classical localized electron pair models. But its bonding and stability can be easily understood using the concept of double aromaticity. There are 28 valence electrons in B_9^-. Sixteen of them are used to form eight 2c–2e σ-bonds between peripheral boron atoms. The remaining 12 electrons are equally split between σ- and π-systems. But they cannot be localized into 2c–2e bonds, neither for the σ- nor π-systems. One can see from Fig. 4 that the delocalized π-electron densities have the same shape as the π-electron densities of benzene, and hence, B_9^- is π-aromatic. However, if we look at the delocalized σ-electrons, they have exactly the same pattern as the π-electrons, except for the nodal plane in the molecular plane. If one accepts π-aromaticity in this cluster, one must accept its σ-aromaticity. This simple bonding picture allows us to understand why we have bond length equalization in this cluster, why it has a ring current similar to benzene, why it has a very large orbital energy gap between its frontier orbitals, and why its first electron detachment energy is high, which are all characteristics of aromaticity. This comprehensive model led to the design and experimental observation of the remarkable wheel-structure of $Ta@B_{10}^-$ clusters (Fig. 5) with the record coordination number of 10 in a planar environment.[74–76] One can see that it is not easy to understand chemical bonding in the $Ta@B_{10}^-$ cluster using canonical MOs (Fig. 5a), but can be easily understood using the concept of double aromaticity (Fig. 5b). The AdNDP analysis determines 10 localized 2c–2e B–B σ-bonds responsible for the B_{10} ring. It also revealed three totally delocalized π-bonds. Interestingly, there are five completely delocalized σ-bonds with 10 electrons, in contrast to the usual three delocalized σ-bonds observed in aromatic molecular-wheel-type planar boron or doped-boron clusters known so far. The 10 delocalized σ-electrons also fulfill the $4n + 2$ Hückel rule for σ-aromaticity. Thus, $Ta@B_{10}^-$ is doubly aromatic, but with a total of 16 delocalized electrons.

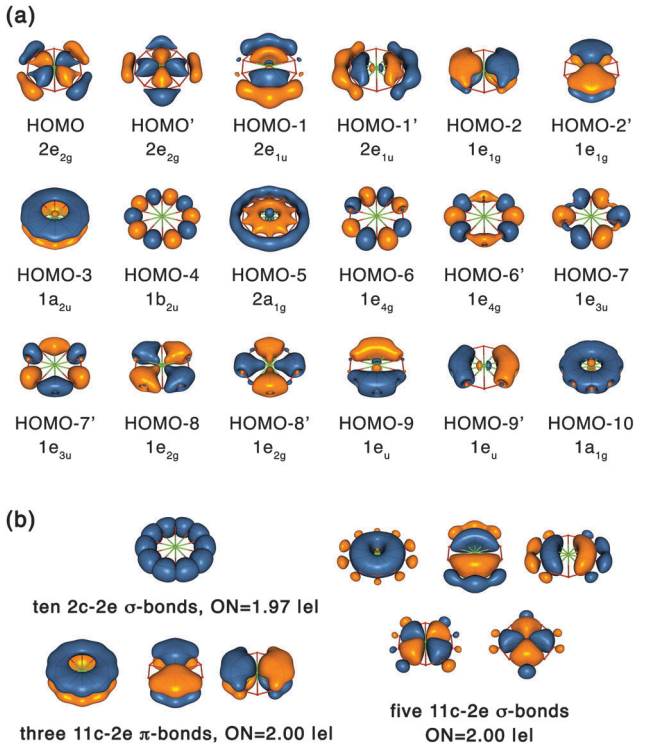

Fig. 5 (a) Molecular orbitals and symmetries of $Ta@B_{10}^-$. (b) AdNDP analysis for $Ta@B_{10}^-$. Reproduced with permission from ref. 76. Copyright 2013, American Chemical Society.

This suggests that the concept of double aromaticity is especially useful in describing chemical bonding in pure and doped boron clusters. In the following section we will describe it in terms of the valence molecular orbitals.

3 The molecular orbitals. Extending Hückel's rules

Let us consider an *n*-membered ring-like molecule of any particular main group atom and assume that all bond lengths of the ring molecule are equal. Now consider the valence s-type atomic orbital and the three p-type molecular orbitals of each of the atoms of our ring-like molecule. The valence molecular orbitals will arise from the linear combination of these atomic orbitals. Imagine, for each of the atoms of the ring, the axis systems depicted in Fig. 6. They will be denoted as π, the one perpendicular to the molecular plane, *t*, the one on the molecular plane and tangential to the ring, and *r*, the one oriented towards the center of the ring in the radial direction.

Now we can build a simplified, but useful, model of the valence molecular orbitals of our *n*-membered ring-like molecule by forming four mutually independent linear combinations of the atomic orbitals lying on each of the three axes. Thus we will end up with four mutually uncoupled sets of molecular orbitals, which will be referred respectively, as the σ_s-type molecular orbitals, the molecular orbitals arising from the linear combinations of the atomic s-type orbitals, the π-type

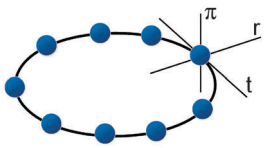

Fig. 6 The three orthogonal axes of each of the atoms of an *n*-membered ring-like molecule.

molecular orbitals, the molecular orbitals arising from the linear combinations of the p-type atomic orbitals lying on the π-axis, the σ_t-type molecular orbitals, the molecular orbitals arising from the linear combinations of the p-atomic orbitals lying on the *t*-axis, and the σ_r-type molecular orbitals, the molecular orbitals arising from the linear combinations of the p-atomic orbitals lying on the *r*-axis.

How the molecular orbitals of each of the four sets will be arranged with respect to their relative energy is determined by the irreducible representations of the point group of the *n*-membered ring-like molecule, namely, the D_{nh} group. The irreducible representations of the D_{nh}, for $n \geq 3$, are at most of dimension two.[77] Hence, the corresponding molecular orbitals will be at most doubly degenerate. Indeed, the resulting energetic ordering is shown in Fig. 7. For *n*-membered rings with *n* even, all the four sets of valence molecular orbitals, *i.e.*: the σ_s set, the π-set, the σ_r-set and the σ_t-set, will be energetically ordered as shown in Fig. 7A, namely, they will come as one nondegenerate molecular orbital above $(n-2)/2$ degenerate molecular orbital pairs which are caped by one non-degenerate molecular orbital at the very top.

Conversely, for *n*-membered rings with *n* odd, the σ_s, π-and σ_r-sets will be ordered as shown in Fig. 7B, with one non-degenerate molecular orbital below $(n-1)/2$ pairs of degenerate molecular orbitals, but the tangential, σ_t, set will be ordered as shown in Fig. 7C, namely, there will be $(n-1)/2$ pairs of degenerate molecular orbitals caped by one non-degenerate molecular orbital.

Naturally, the number of nodes of the molecular orbitals increases as one increases in energy. It should not be stated for sure, but as a rule of thumb we can assume that those molecular orbitals having fewer nodes will be occupied preferentially. Consequently, the occupation of the molecular orbitals of each set will depend on their relative energies with respect to those of the other sets. This constitutes the physical basis of the *multiple-fold* aromaticity concept, namely, the simultaneous occurrence of more than one set of valence molecular orbitals

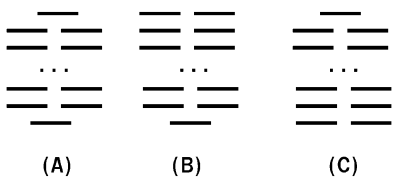

Fig. 7 Three types of energetic orderings of the valence molecular orbitals of *n*-membered ring-like molecules. (A): *n* even. (B): *n* odd, radial like. (C): *n* odd, tangential like.

each of them conforming to $(4n+2)$, $n \in \mathcal{N}$, Hückel's electron counting rule.

This scheme can naturally be extended to d- and f-type atomic orbitals. The resulting combinations of the d-orbitals will be grouped into σ_r, σ_t, π_r, π_t and δ-type molecular orbital sets. Finally, the f-atomic orbitals will form σ_r, σ_t, π_r, π_t, δ_r, δ_t and ϕ-type molecular orbitals. A detailed description of these molecular orbital sets can be found elsewhere.[52,78]

With this scheme at hand one has now to count the number of valence electrons of the molecule and place them into the corresponding molecular orbitals, observing both, the Aufbau principle and Hund's rule. This will yield an approximate, albeit appealing picture of the electronic structure of the *n*-membered ring molecule of interest.

3.1 σ–π-Aromaticity in the Al_4^{2-} cluster

The tetra-aluminum dianion, Al_4^{2-}, was isolated in Wang's laboratory at PNNL, Richland, WA, as a bimetallic charge-compensated system of composition MAl_4^-, with M = Li, Na, or Cu. Wang and co-workers reported photoelectron spectra of bare $CuAl_4^-$, $LiAl_4^-$, and $NaAl_4^-$ clusters claiming that the planar square structure of the Al_4^{2-} cluster, a building block of all these clusters, is aromatic.[79,80] It was found computationally that $CuAl_4^-$, $LiAl_4^-$, and $NaAl_4^-$ clusters have pyramidal structures (Fig. 8) with the planar square of Al_4^{2-} being a base of these pyramids. Comparison of calculation results and experimental photoelectron spectra confirmed these theoretical findings. Furthermore, the search for the global minimum of the metastable Al_4^{2-} cluster revealed that the planar square structure was actually the lowest in energy. It is not stable with respect to an electron detachment, but when a compact basis set is used the obtained electronic structure is consistent with its electronic structure in the singly charged $CuAl_4^-$, $LiAl_4^-$, and $NaAl_4^-$ clusters (Fig. 8b and c). Detailed discussion of this issue can be found in ref. 81. The question is why the Al_4^{2-} cluster adopts this high symmetry structure? The answer is because this dianion is doubly σ- and π-like aromatic. Indeed, four lowest canonical MOs go to form four lone pairs with one located on every aluminum atom and do not participate in chemical bonding. Three other MOs are responsible for bonding in this cluster. The HOMO is a completely bonding π-MO. Two electrons on that MO make this cluster π-aromatic. The HOMO−1 is a completely bonding MO formed by radial p_σ-AOs. Two electrons on that MO make this cluster σ_r-aromatic. The HOMO−2 is a completely bonding MO formed by tangential p_t-AOs. Two electrons on that MO make this cluster σ_t-aromatic. Thus, this is an example of a system with double (σ- and π-like) and threefold (σ_r, σ_t and π) aromaticity. These three molecular orbitals, that contribute to the chemical bonding in Al_4^{2-}, are orthogonal to each other since they are formed from linear combinations of atomic orbitals of different symmetries. Conversely, each of them can be expressed as linear combinations of four localized bonding orbitals, as elegantly put forward by Dixon *et al.*[82] The implication of this is that each of three delocalized bonding molecular orbitals has four independent resonant structures. Consequently, the valence

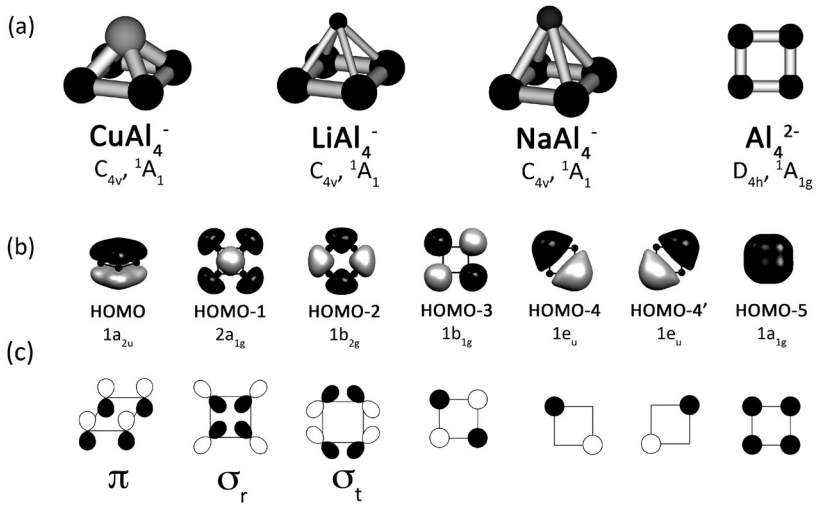

Fig. 8 The global minimum structures of the MAl_4^- clusters (M = Cu, Li, and Na) and the isolated Al_4^{2-} cluster (a); valence canonical molecular orbitals (CMOs) of the isolated Al_4^{2-} cluster (b); schematic representation of valence CMOs as linear combinations of four $3p_z$ atomic orbitals (AOs) comprising the highest occupied molecular orbital (HOMO), four 3p-radial AOs (HOMO−1), four 3p-tangential (HOMO−2), as well as four different linear combinations of 3s AOs (HOMO−3, HOMO−4, HOMO−4′, and HOMO−5). Reprinted with permission from ref. 54. Copyright 2012 Copyright Clearance Center.

bond representation of the chemical bonding in Al_4^{2-} involves $4 \times 4 \times 4 = 64$ resonating Kekulè structures. Naturally, not them all will have the same weight. In particular, it was anticipated[82] that a full valence bond calculation with all these 64 resonating structures will show that the resonating structures associated with triple Al–Al bonds will have a very small weight. Kuznetsov *et al.*[80] eliminated also the resonant structures featuring π Al–Al bonds with no σ-bonds between the same pair of atoms, resulting all together in 12 resonant structures. Finally, Havenith and van Lenthe[83] carried out *ab initio* valence bond calculations and found that the bonding structure of Al_4^{2-} can be described with 6 main resonant structures, four Kekulè like and two Dewar like (diagonal bonding). Surprisingly, the Dewar ones have the largest weights.

Altogether, it is worth noticing that benzene has (only) two main resonant Kekulè structures. The large number of resonance structures of Al_4^{2-} accounts for its large resonance energy, RE,

$$\mathrm{RE}(Al_4^{2-}) = \Delta E(Al_4^{2-} \rightarrow 4Al + 2e^-) - 3 \times \Delta E(Al_2(^1\Sigma_g) \rightarrow 2Al) \quad (1)$$

estimated as the difference in the atomization energy of Al_4^{2-} and the dissociation energy of three localized Al–Al bonds, because Al_4^{2-} has three bonding electron-pairs. High level *ab initio* calculations of Dixon *et al.*,[82] based on extrapolating the computed CCSD(T)/aug-cc-pVxZ (x = D, T, and Q) resonance energies to the complete basis set limit, yielded $\mathrm{RE}(Al_4^{2-}) = 72.7$ kcal mol^{-1}. Notice that in eqn (1), the lowest lying singlet $^1\Sigma_g$ of Al_2 has been taken as the reference state for the localized Al–Al bonds. However, when the $^3\Pi_u$ ground state of Al_2 is taken as the reference state, the resonance energy of Al_4^{2-} turns out to be 52.5 kcal mol^{-1}. The latter estimate is closer to the average resonance energy of 48 kcal mol^{-1} calculated by Boldyrev and Kuznetsov[84] from the atomization energy of the Na_2Al_4 cluster referred to a system with two Na–Al interactions and three Al–Al bonds. Finally, Havenith and van Lenthe[83] were able to calculate the resonance energies of the σ- and π-systems of Al_4^{2-} by means of their *ab initio* valence bond calculations. They found that the σ-system, which is composed of the two independent radial and tangential systems each containing two delocalized electrons, has a resonance energy significantly higher than that of the π-system (123 *vs.* 40 kcal mol^{-1}). Noteworthily, the π-resonance energy of Al_4^{2-} is substantially lower than that of its π-isoelectronic hydrocarbon $C_4H_4^{2+}$ (167 kcal mol^{-1}). Follow-up theoretical studies agree with the overall assignment of this cluster as aromatic. Additionally, it has also been shown that it is more σ-, than π-aromatic.[82,84–92]

Antiaromaticity as introduced by Breslow is due to the destabilization of cyclic systems with $4n$ π-electrons by Jahn–Teller distortion, yielding antiaromatic species that are more reactive than their nonaromatic counterparts. Cyclobutadiene is a prototypical antiaromatic molecule with rectangular structure. From the joint photoelectron and theoretical study of the $Li_3Al_4^-$ cluster it was shown[93] that it contains an approximately rectangular Al_4^{4-} kernel and its Vertical Electron Detachment Energy (VEDE) 1.39 eV is appreciably lower than VEDE = 2.15 eV of the aromatic $LiAl_4^-$ cluster. It was said to be an example of the net all-metal antiaromatic species (Fig. 9).

MO analysis revealed that the $Li_3Al_4^-$ cluster is σ-aromatic and π-antiaromatic (Fig. 9). The $Li_3Al_4^-$ cluster has 8 valence electron pairs. Four of them are responsible for the formation of four lone pairs (one pair on every aluminum), two MOs (HOMO−1 and HOMO−2) are responsible for $\sigma_{r-} + \sigma_{t-}$ aromaticity similar to Al_4^{2-}, and two MOs (HOMO and HOMO−4) are responsible for π-bonding, and since there are four π-electrons, the $Li_3Al_4^-$ cluster is π-antiaromatic. The assignment of this cluster to net antiaromaticity created a controversy in the literature. Everybody agrees that the $Li_3Al_4^-$ cluster is σ-aromatic and π-antiaromatic but disagrees on the net antiaromaticity (see the discussion about that in ref. 22).

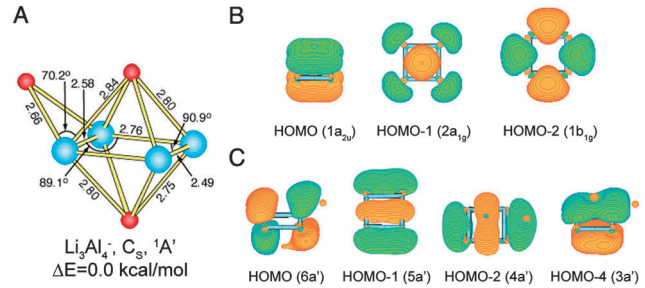

Fig. 9 (A) Optimized global minimum structure of $Li_3Al_4^-$; bond lengths in angstroms. Molecular orbital pictures: (B) Al_4^{2-}; (C) capped octahedral structure of $Li_3Al_4^-$. Adapted with permission from all-metal antiaromatic molecule: rectangular Al_4^4 in the Li_3Al_4 Anion, Aleksey E. Kuznetsov, K. Alexander Birch, Alexander I. Boldyrev, Xi Li, Hua-Jin Zhai, and Lai-Sheng Wang, *Science*, 2003, **300**, 622. Copyright 2003, American Association for the Advancement of Science.

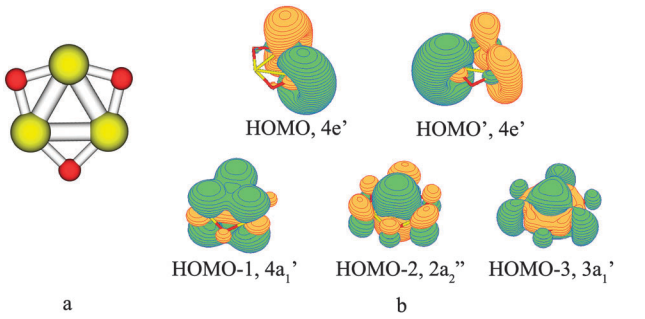

Fig. 10 Global minimum structure (a) and five upper valence MOs (b) of $Ta_3O_3^-$ adapted with permission from Hua-Jin Zhai, Boris B. Averkiev, Dmitry Yu. Zubarev, Lai-Sheng Wang, Alexander I. Boldyrev. Ît′ Aromaticity in $[Ta_3O_3]^-$, *Angew. Chem., Int. Ed.*, 2007, **46**, 4277 (ref. 97). Copyright Wiley-VCH Verlag GmbH & Co. KGaA.

3.2 σ–π–δ-Aromaticity in transition metal clusters

Aromaticity has been recently extended to transition metal, which allows δ-aromaticity/antiaromaticity as it was postulated by Boldyrev and Wang in 2005.[22] Wang and co-workers[46] discovered the first d-AO based σ-aromaticity in the suboxide $M_3O_9^-$ and $M_3O_9^{2-}$ (M = Mo and W) clusters. The d-AO σ-aromaticity was recently extended from clusters in a molecular beam to solid state compounds, such as $(LAu_3)^+$ (L = 1,3-bis(2,6-diisopropylphenyl)-imidazol-2-ylidene),[94] $[Zn_3Cp_3]^+$ and $[Zn_2CuCp_3]$.[95]

Chi and Liu reported first examples of d-based double (σ- and π-) aromaticity in bare X_3^- (X = Sc, Y, and La) clusters.[96] According to their calculations 2a′- and $1a_2''$-MOs (both formed by d-AOs of transition-metal atoms) are responsible for delocalized bonding in equilateral triangular global minimum structures of X_3^-.

Zhai *et al.*[97] reported the first example of δ-aromaticity in a $Ta_3O_3^-$ cluster. The global minimum $Ta_3O_3^-$ structure has a singlet state with three Ta atoms forming an equilateral triangle geometry and oxygen atoms occupying the bridge positions (Fig. 10). If we assume that the oxidation state of oxygen is −2, then the formal oxidation state of Ta is +1.66 leaving 10 electrons for direct metal–metal bonding. Among all five upper MOs, delocalized σ-bonding is canceled since the doubly degenerate bonding/antibonding-HOMO (4e′) and completely bonding HOMO−3 ($3a_1'$) are completely occupied and thus the σ-bonding character of HOMO−3 is canceled by the antibonding nature of HOMO. The HOMO−1 is a completely bonding δ-MO and HOMO−2 is a completely bonding π-MO and thus this cluster is doubly (δ- and π-) aromatic according to the $(4n + 2)$ rule for aromaticity in the cyclic systems with $n = 0$ applied separately to δ- and π-electrons.

Averkiev and Boldyrev[48] found that the Hf_3 cluster in the lowest $^1A_1'$ (D_{3h}) state is the first example of triple (σ-, π- and δ-) aromaticity (Fig. 11). Using the AdNDP analysis, they showed that Hf_3 in the singlet state has three 2c–2e Hf–Hf σ-bonds formed by hybrid 6s-, 5d-AOs and three completely delocalized bonds formedby pure d-AOs (one completely bonding 3c–2e d-radial based σ-bonds, one completely bonding 3c–2e d-radial based π-bonds, and one completely bonding 3c–2e d-AO based

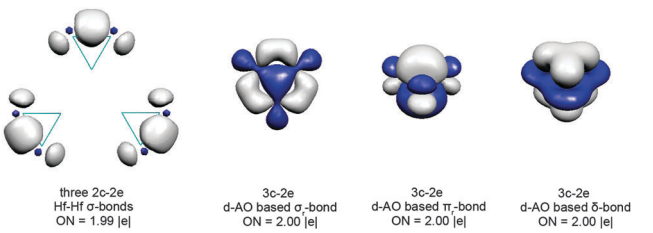

Fig. 11 The three 2c–2e Hf–Hf σ-bonds, 3c–2e d-AO based δ-bonds, 3c–2e d-AO based π_r-bonds, and 3c–2e d-AO based δ-bonds revealed by the AdNDP analysis at B3LYP/LANL2DZ for the triply σ-, π- and δ-aromatic Hf_3 ($^1A_1'$, D_{3h}) cluster. Hf–Hf distance R = 2.734 Å. (Reprinted with kind permission from Springer Science + Business Media, ref. 52, Copyright 2010 Springer-Verlag Berlin Heidelberg.)

δ-bonds). The 3c–2e d-AO based δ-bond is formed by the overlap of the d_{z^2} atomic orbital on each Hf atom. These three delocalized bonds are responsible for the presence of triple aromaticity.

While everyone would expect that δ-aromaticity would be weaker than σ- and π-aromaticity bonding-wise, high symmetry is still expected for δ-aromatic compounds. Probably the most remarkable example of δ-aromaticity responsible for bonding and structure of the transition metal cluster is the compound containing the $[Pd_4(\mu_4\text{-}C_9H_9)(\mu_4\text{-}C_8H_8)]^+$ triple-decker sandwich complex synthesized and characterized by Murahashi *et al.*[98] Sergeeva and Boldyrev[99] performed the AdNDP analysis of chemical bonding in the $[Pd_4(\mu_4\text{-}C_9H_9)(\mu_4\text{-}C_8H_8)]^+$ triple-decker sandwich complex and showed that the Pd_4 core resembles an almost perfect square due to δ-aromaticity.

3.3 σ–π–δ–ϕ-Aromaticity in lanthanoid clusters

Tsipis *et al.*[100] have discussed the ϕ-aromaticity of a number of lanthanoid clusters $[c\text{-}Ln_3]^{+/0/-}$, with Ln = La, Ce, Pr, Nd, Gd, and Lu. They have determined through DFT calculations that all these clusters have a perfect D_{3h} three-membered ring like ground state, very stable towards full atomization. Analysis of their valence molecular orbitals revealed that largely delocalized orbitals of σ-, π-, δ- and ϕ-symmetry were involved in the bonding. Although it should be taken with caution (see ref. 101 and 102),

the calculated out-of-plane Nucleus Independent Chemical Shift, $NICS_{zz}$ (see Section 4), at the center of the three-membered ring, and at 1 Å above it, revealed a magnetic diatropic response associated with aromaticity (see Section 4) for $[c\text{-}Lu_3]^{+/0}$, while $[c\text{-}La_3]^{+/0/-}$ yields a small paramagnetic local response, and hence, suggests that the La cluster is weakly antiaromatic, irrespective of its charge state. Subsequently, the latter clusters have been used to model the electronic structure of $La_3@C_{110}$ and $Lu_3@C_{80}$ endohedral metallofullerenes. For instance, Tsipis and Gkekasa[103] have found that the $[Cp_3Ln_3(\mu_2\text{-}H)_3]^{+/0}$ (Ln = La and Lu; Cp = $C_5H_5^-$) clusters are very reactive towards H_2, HX (X = F, Cl, Br, and I), O_2 and N_2. However, both clusters retain their structural integrity upon reaction.

All in all, studies on ϕ-(anti)aromaticity derived from the delocalization of f-type atomic orbitals are in their infancy. Consequently, both theoretical and experimental studies are further required to make progress in the field. Clearly, understanding the (anti)aromaticity of metal, including lanthanoid and heavier elements, compounds constitutes the next frontier in inorganic chemistry. Additional calculations on f-block ring like clusters can be found elsewhere.[104,105]

4 The magnetic criteria and electron density analysis of aromaticity in all-metal clusters

In planar aromatic ring-like molecules, an externally applied magnetic field will produce a ring current due to the mobility of the aromatic ring delocalized electrons. This induced ring current will subsequently generate an induced magnetic field, which in accordance with Biot-Savat's law will oppose the externally applied magnetic field. Both the induced ring current and the induced magnetic field can be estimated theoretically and constitute a probe for the aromaticity/antiaromaticity of the system under study.[106,107]

The magnetic response properties of Al_4^{2-} have been extensively studied in the past and a consensus has been reached on the fact that the magnetic criteria support the presence of double, σ- and π-aromaticity in Al_4^{2-}. Thus, Fowler *et al.*[88,89] computed the current–density maps *via* coupled Hartree–Fock perturbation theory in the continuous transformation of the origin current–density diamagnetic zero (CTOCD-DZ) formulation. They found significant differences from conventional carbon-based aromatic systems. The delocalized diamagnetic current induced by a perpendicular magnetic field is carried by the σ- and not by the π-electrons, and this remains so whether the aluminum square is isolated or forming part of a bimetallic cluster. In other words, the π-orbital is magnetically inactive in Al_4^{2-}. This magnetic behavior is in sharp contrast to the active role of the two π-electrons in $C_4H_4^{2+}$. Havenith *et al.*[90] also mapped the current density of $Li_3Al_4^-$ using the CTOCD-DZ method. The current in this 4π-system is diatropic in the plane but paratropic out of the plane. They suggested that a description of four-electron σ-diatropic/two-electron π-paratropic seems to be more appropriate for the chemical bonding of this cluster.

The aromatic ring current shielding (ARCS) approach[108] is a method to determine the strength of the induced ring current, which is related to the molecular aromaticity. In the ARCS method, the strength of the induced aromatic ring current and the size of the current ring are obtained from nuclear magnetic shielding constants calculated in a discrete number of points along a line perpendicular to the molecular plane starting at the center of the molecule. The ARCS calculations show that the Al_4^{2-} ring sustains in magnetic fields a strong diatropic ring current of about 9–12 nA T^{-1}. For comparison, the ring-current susceptibility for benzene[86] is about 8 nA T^{-1}.

Magnetically induced current density in Al_4^{2-} and Al_4^{4-} species was computed at the CCSD level of theory by applying the gauge-including magnetically induced current (GIMIC) method.[109] The strength of the ring-current susceptibilities was obtained by numerical integration of the current densities passing through a cross-section perpendicular to the Al_4 ring.[87] The GIMIC computations support that Al_4^{2-} sustains a net diatropic ring current. The diatropic contribution to the ring-current susceptibility is carried by the electrons in both the σ (16.7 nA T^{-1}) and π-orbitals (11.3 nA T^{-1}). The induced ring current in Al_4^{4-} consists of about equally strong σ-diatropic and π-paratropic currents of about 14 and −17 nA T^{-1}, respectively. The net current susceptibilities obtained for $LiAl_4^-$, Li_2Al_4, $Li_3Al_4^-$, and Li_4Al_4 are 28.1, 28.1, −5.9, and −3.1 nA T^{-1}, respectively.

In 2003, Chen *et al.*[91] revisited the antiaromatic character of $Li_3Al_4^-$ using the nucleus independent chemical shift (NICS) analysis.[110] NICS corresponds to the negative of the magnetic shielding computed at chosen points in the vicinity of molecules. NICS is normally computed at ring centers, at points above, and even at grids of points located in and around the molecule. Significantly negative (or magnetically shielded) NICS values in interior positions of rings or cages indicate the presence of induced diatropic ring currents or ''aromaticity'', whereas positive values (or deshielded) at each point denote paratropic ring currents and ''antiaromaticity''. Several modifications of NICS exist, of which one separates the total into contributions from canonical molecular orbitals (CMO-NICS). CMO-NICS analysis of two-π-electron Al_4^{2-} confirms that not only the diatropic π (−17.8 ppm) but also the σ-MOs (−11.1 ppm) contribute importantly to aromaticity. In contrast, the four π-electron system of $Li_3Al_4^-$ is paratropic (14.2 ppm), conforming to the Hückel rule. However, NICS indicates that this π-antiaromaticity is overcome by the diamagnetic contributions of all σ-orbitals put together (−16.8 ppm).

In 2006, Havenith and Fowler[92] discussed the apparent contradictions between ipsocentric, NICS, and GIMIC evaluations of ring-current aromaticity in Al_4^{2-}. They argued that the out-of-plane component of π-shielding is small, as is consistent with the small π-contribution to ring current. In contrast, the in-plane component of σ-shielding is large, as is consistent with the significant NICS(0) value. In principle, there is no essential disagreement between current density maps and NICS(0). On the contrary, the tensor component that is directly connected to ring current shows that the aromaticity of Al_4^{2-} is

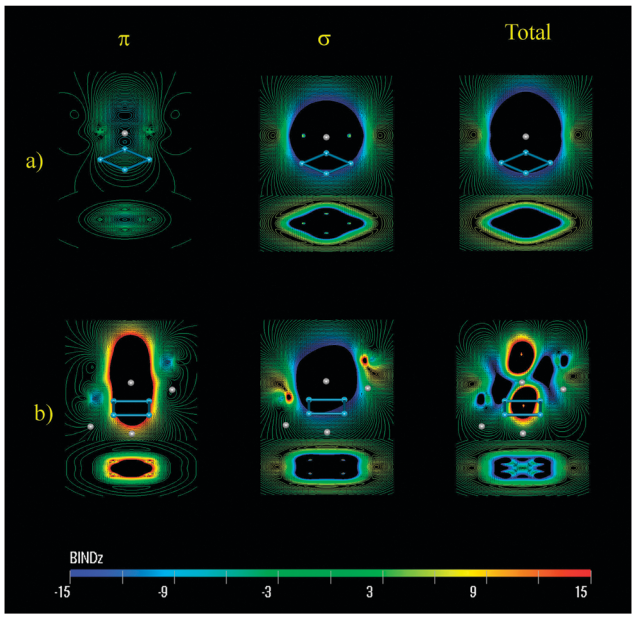

Fig. 12 Isolines of B_z^{ind} in (a) Al_4Li^- and (b) Al_4Li_4. The scale is given in ppm or μT for an external field of 1 T. Reproduced with permission from ref. 112. Copyright 2012, American Chemical Society.

σ- and not π-based. In this respect, the authors wrote: "... a measure such as $NICS_{zz}(0)$ would presumably be a better reflection of aromaticity on the magnetic criterion".

In 2007, Islas *et al.*[111] showed that Al_4^{2-} and Al_4^{4-} cannot be discussed isolated from the counterions: the cations not only stabilize the aluminum square electrostatically but also have an influence on the chemical structure. Molecular dynamics simulations indicate that the cations are relatively fixed for $LiAl_4^-$ and Li_2Al_4, but become more floppy for $Li_3Al_4^-$ and Li_4Al_4. So, for the 4π cases any static structural representation is not realistic at all. Magnetically, the induced magnetic field representation (see Fig. 12) agrees with the former investigations of Al_4^{2-} based on NICS and GIMIC concerning the σ- and π-system.[112] For the total response, the B_z^{ind} computations (B_z^{ind} and $NICS_{zz}$ are the same) show that a simple classification of a molecule as "aromatic" or "antiromatic" is impossible for those systems containing a Al_4^{4-} backbone. For such cases, the complete map of the induced magnetic field shows the "bitropic" character of the cluster, the diatropic contribution raised by the σ-electrons, which dominates in the ring plane, and the paratropic part, induced by the π-system around the *z*-axis.

Solà and co-workers computed the NICS profiles for a large series of inorganic rings. They show that all NICS minima neither fall near the ring center, nor are located at 1.0 Å of it. Therefore, the widespread NICS(0) and NICS(1) values used in organic molecules to diagnose aromaticity are not necessarily the best option for all-metal systems. NICS profiles are highly dependent on the size ring, the kind of aromaticity present, and the nature of the atoms involved. The reliability of negative NICS values to assess aromaticity has been further analyzed by Foroutan-Nejad *et al.*[101] for transition metal clusters. They have found that in these clusters negative NICS values originate from localized strong paramagnetic current around the atomic nuclei, but an in-depth analysis of the current density shows that they do not sustain a diamagnetic ring current and consequently cannot be classified as aromatic clusters. The conclusion is that NICS should be carefully scrutinized before classifying transition metal clusters as aromatic.[102] Analysis of current densities is recommended over NICS for the determination of aromaticity in transition metal clusters.

Finally, studies of the electron density and associated scalar fields of Al_4^{2-} have also been carried in order to ascertain the nature of its chemical bonding. Thus, Fias *et al.*[113] studied the so-called linear response kernel to gain insights into the aromatic behavior of Al_4^{2-}. When at a given point, *r*, a positive change, $\delta v(r)$, in the potential is induced (leading to a more positive potential at that point), electron depletion occurs in the immediate neighborhood around the point *r*. Depending on how much delocalized the electron density of the molecular system is around *r*, the response is more or less localized around the point of the perturbation. The unintegrated plots of the linear response function of Al_4^{2-} clearly show the delocalized nature of the response in this cluster. The response is more pronounced in the σ-electron density than in the π-density, pointing out that the system is mainly σ-aromatic.

Santos *et al.*[85] suggested an orbital partition of the electron localization (ELF) function in order to diagnose aromaticity. The ELF, defined originally by Becke and Edgecombe[114] as a measure of electron localization, clearly shows the separation between the core and valence electrons, and also between bonding and lone electron pairs.[115,116] Interestingly, it has recently been reported that Al_4^{2-} presents a surprisingly high ELF_π (the ELF built using only the π-orbitals) bifurcation value of 0.99, which is even higher than the value associated with benzene.[117] This anion also shows a high bifurcation value for the ELF_σ (0.88), which agrees with the prediction of a strong σ-delocalization. The analysis of this scalar field was also applied to $Li_3Al_4^-$ and Li_4Al_4, indicating an overall antiaromatic character for Al_4^{4-} based structures, built from σ-aromatic and π-antiaromatic contributions.

5 Functionalization of all-metal aromatic clusters

We finished Section 3.2 commenting upon the remarkable structure of the $[Pd_4(\mu_4\text{-}C_9H_9)(\mu_4\text{-}C_8H_8)]^+$ triple-decker sandwich complex, and in particular emphasizing that the perfect square geometrical arrangement of the middle Pd_4 deck should be ascribed to its δ-aromaticity. Indeed, the palladium tetramer can be formally best seen as Pd_4^{2+} and the two capping ligands as the 10 π-electron aromatic $C_9H_9^-$ and 8 π-electron antiaromatic C_8H_8 ligands, respectively. Thus, aromaticity/antiaromaticity appears in all the three decks of the complex.

Consequently, it seems legitimized to hypothesize whether aromatic all-metal clusters could also be used as capping ligands to form sandwich complexes, in such a way that upon complex formation charges are partitioned among the

various decks so that all-metal cluster capping ligands result to be aromatic.

This idea was tested by Mercero *et al.*[118] who reported computational evidence of the stability of the $[Ti(\eta^4Al_4)_2]^{2-}$ sandwich complex. An in-depth analysis of its molecular orbitals along with their associated NICS values concluded that the three-fold aromatic nature of both Al_4^{2-} ligands remains intact upon complex formation. Although this complex was found to be unstable towards electron autodetachment, it was demonstrated that alkali counterions could stabilize it. These studies were later extended to all the transition metal elements,[119] providing a guide for experimental studies of these novel sandwich complexes.[22,49] All data discussed in this section have been computed at the B3LYP/TZVP+G(2df,2p) level of theory (see ref. 120 for a full account of the theoretical methods used).

However, in spite of the thermodynamical stability of these sandwich complexes, their kinetic stability was found to be very weak. Thus, Sun and co-workers[121] established that such complexes, if synthesized, will collapse rapidly into larger clusters with an increased number of Al–Al contacts. Indeed, such an aggregation of aluminum small rings into larger clusters was precluded earlier by Seo and Corbett,[122] who emphasized that the kinetic stability of compounds containing Al rings will largely be determined by putting them as far apart from each other as possible. The "unprotected" aluminum atoms in $[Ti(\kappa^4Al_4)_2]^{2-}$ are indeed very prone to aggregation as demonstrated by the quantum molecular dynamics simulation of the Na^+ stabilized $[Ti(\kappa^4Al_4)_2]^{2-}$ complex shown in Fig. 13. The complex is seen to have a very short lifetime of less than 2.0 ps at room temperature. Then, it collapses into an aggregated structure which remains stable for the rest of the simulation time.

In this vein, functionalization of the aluminum atoms of the ring by attaching covalent ligands turns out to be desirable for it will serve two purposes, namely, it will separate the aluminium atoms from each other and will protect the aluminum atoms against aggregation. Additionally, attaching (bulky) substituents will also provide anchoring sites to fix the Al rings into large molecular species.

This possibility was made real by Power *et al.* who synthesized the $Na_2[Al_3R_3]$, R = 2,6-dimesitylphenyl complex, (see Fig. 14 and ref. 123). A preliminary inspection of the calculated valence molecular orbitals of this complex by the same authors revealed an occupied π-type orbital, delocalized over the three aluminum atoms, which led them to state that... "$Na_2[Al_3R_3]$ '*is aromatic*', in accordance with Hückel's $(4n + 2)$ rule".

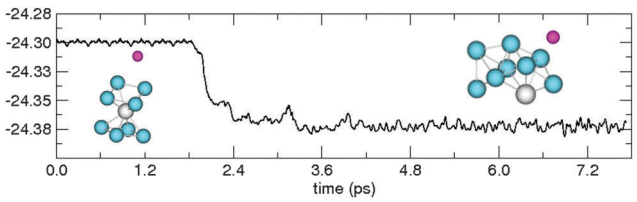

Fig. 13 The energy of $Na[Ti(\kappa^4Al_4)_2]^-$, in eV, as a function of the simulation time in picoseconds. Cyan: Al, grey: Ti, and magenta: Na.

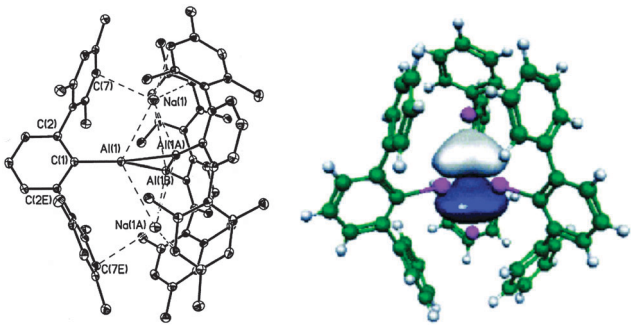

Fig. 14 Left, thermal ellipsoid plot (30% probability) of $Na_2[Al_3R_3]$, R = 2,6-dimesitylphenyl without H atoms. Selected bond lengths [Å] and angles [deg]: Al(1)–Al(1A) 2.520(2), Al(1)–C(1) 2.021(3), Al(1)–Na(1) 3.285(2), Na(1)–C(7) 3.066(2), Na–C_{ring} 3.066(2)–3.808(2) [av. 3.459(2)], Mes(centroid)–Na(1A) 3.177(2); A1(1)–Al(1A)–Al(1B) 60.0, Al(1A)–Na(1)–Al(1B) 45.12(3), C(1)–Al(1)–Al(1A) 142.8(1), C(1)–Al(1)–Al(1B) 157.2(1). Dihedral angle between the Al_{i3} plane and the Na(1)–Al_3(centroid)–Na(1A) plane: 90.0. Mes = C_6H_2-2,4,6-Me_3. Right, Kohn–Sham orbital representation for the delocalized HOMO−2 of $Na_2[(AlAr)_3]$ (Ar = C_6H_3-2,6-Ph_2). Reproduced with permission from ref. 123. Copyright 2006, Wiley-VCH.

The aromaticity of the $[Al_3R_3]^{2-}$ cluster was further examined by Mercero *et al.*,[124] who established that its fourteen valence electrons are arranged as shown in Fig. 15. Consequently, the cluster is σ- and π-aromatic in accordance with Hückel's rule as applied to each of the valence molecular orbital sets. This agrees with the calculated NICS at the center of the ring, NICS(0) = −13.04 ppm, and at 1 Å above the center of the ring, NICS(1) = −11.02 ppm. The former is an indicator of σ-aromaticity and the latter of π-aromaticity. Nonetheless, a deeper analysis of the magnetic responses of the valence molecular orbitals through the inspection of CMO-NICS, revealed that the ψ_t system is antiaromatic in $[Al_3H_3]^{2-}$, as shown by their positive CMO-NICS values reported in Fig. 15. However, it was also found in the same research that the aromaticity of the $[Al_3R_3]^{2-}$ cluster depends markedly on the nature of the R substituent. Thus, it was found that both π-acceptors, like –C≡N, and σ-donors, like $–CH_3$, increase the aromaticity of the cyclotrialane ring, relative to that of $[Al_3H_3]^{2-}$. But the largest enhancement

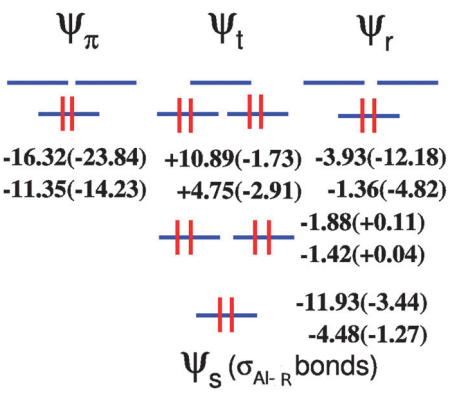

Fig. 15 CMO-NICS, in ppm, analysis at the ring center (top number of each of the pairs) and at 1 Å above the ring center (bottom number of each of the pairs) of $[Al_3H_3]^{2-}$ and of $[Al_3F_3]^{2-}$, in parentheses. Reproduced with permission from ref. 124. Copyright 2009, American Chemical Society.

of the aromaticity of the ring occurs for halides. In particular, $[Al_3F_3]^{2-}$ was predicted to be highly aromatic as suggested by its large negative NICS values, NICS(0) = −45.14 ppm and NICS(1) = −27.61 ppm. Observe, see Fig. 15, that for $[Al_3F_3]^{2-}$, even the tangential degenerate molecular orbitals are slightly aromatic, opposite to their noticeable antiaromaticity in $[Al_3H_3]^{2-}$.

Voluminous substituents, R, at the Al_3R_3 rings, have, indeed, been used to protect aluminum atoms from collapsing and to provide isolation. Thus, Schnöckel *et al.* have succeeded to crystallize the $[Al(\eta^3Al_3R_3)_2]^-$, R = $N(SiMe_3)_2$[125] and $[Al(\eta^3Al_3R_3)_2]^\bullet$, R = $N(SiMe_2Ph)_2$,[126] sandwich complexes, see Fig. 16. However, after a careful study of the electronic structure of the $[Al(\eta^3Al_3H_3)_2]^-$ *model compound*, they concluded that the $[Al_3R_3]^{2-}$ ligands should not be described as aromatic systems because of the lack of a ring-current-induced high field shift for the central Al. Namely, the calculated ring-current-induced field shift at the central Al is δ(Al) = +798 ppm in $[Al(\eta^3Al_3H_3)_2]^-$, which should be compared with the value of δ(Al) = −114 ppm induced by *real* aromatic rings, like in the aluminocenium $[Al(\eta^5Cp^*)_2]^+$ cation.[127] The calculated NICSs, at the center and at 1 Å above the plane of the $[Al_3R_3]^{2-}$ rings in $[Al(\eta^3Al_3H_3)_2]^-$, NICS(0/1) = −1.34 ppm/−6.47 ppm, indicate that the aromaticity of the $[Al_3H_3]^{2-}$ ligands decreases substantially upon complexation, in accordance with the prediction of Schnöckel *et al.*[126] Although, given the strong dependence of the aromaticity of the $[Al_3R_3]^{2-}$ ligands with respect to the nature of the substituent R, it should be plausible to find out substituents R that protect the aluminium atoms from collapsing and at the same time retain the aromaticity of the ligands upon complexation. It is anticipated that finding such ligands will be a challenging task.[128]

Similarly one could also functionalize Al_4^{2-} to yield stable aromatic $Al_4R_4^{2-}$ species. Indeed, the recent discovery and subsequent structural characterization[129,130] of the Al_nH_{n+2}, $4 < n < 8$ closo-alanes, have certainly opened a new chapter on aluminum hydride chemistry. Assisted by the extension of the Wade–Mingos rules and their underlying Polyhedral Skeletal Electron Pair (PSEP) theory,[131,132] Schnöckel *et al.*[130] have nicely accounted for the closo-polyhedra structures of their recently synthesized closo-alanes, in consonance with their borane analogs. The analogy between the alanes and the boranes is such that even the well-known *tetrahedral exception* to the Wade–Mingos rules for closo-boranes does also apply to the closo-alanes, and rationalizes the experimentally found structure of Al_4H_6, whose $Al_4H_4^{2-}$ core distorts from its Wade–Mingos T_d structure to a D_{2d} one, aided by the stabilizing field exerted by the remaining two protons.

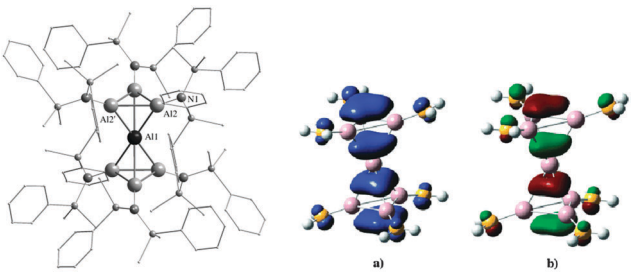

Fig. 16 Left, the molecular X-ray crystal structure of $[Al_7\{N(SiMe_2Ph)\}_6]$. The Al1–Al2 bond length (the distance between the central and each of the six symmetry-equivalent Al atoms) is 2.73 Å. The Al–Al bond length in the Al_3 rings (Al2–Al2′) is 2.61 Å. All Al–N bond lengths are 1.81 Å. The environment of each N atom is planar (sum of angles = 360 deg.). The N–Si bond length is 1.75 Å. Right, (a) the Kohn–Sham spin-density and (b), the Kohn–Sham SOMO (a_{2u}) of the $[Al_7\{NH_2\}_6]$ model compound. Reproduced with permission from ref. 126. Copyright 2007, Wiley-VCH.

Fig. 17 The structure of $E^+\cdot[Al_4H_4]^{2-}\cdot E^+$, left, and of $E^+\cdot[Al_4H_4]^{2-}$, right. E = Li and Na. Cyan: Al, grey: H, and magenta: E.

Table 1 Electron detachment energies, EDE, in eV for $Na^+\cdot[Al_4H_4]^{2-}$

MO	Symmetry	EDE	Pole strength
HOMO	a_1	2.541	0.884
HOMO−1	b_1	2.008	0.853
HOMO−2 & −3	e	3.657	0.814

However, when the two additional protons are replaced by alkali cations like Li^+ or Na^+, the distortion of the Wade–Mingos tetrahedra process further till the planar D_{4h} symmetry structure, yielding an inverted sandwich coordination complex $E^+\cdot[Al_4H_4]^{2-}\cdot E^+$, with E = Li and Na, shown in Fig. 17, which is stable towards both geometrical distortions and electron autodetachment.

The integrity of the $Al_4H_4^{2-}$ species has been investigated further and found that it is a structurally stable chemical species with no negative force constants. This dianionic molecule, however, is prone to electron detachment, but it can be stabilized with either two, as mentioned above, and even only one alkali cation. Thus, we show below in Table 1, the characterized $^1A_1$ ground state of the C_{4v} $Na^+\cdot[Al_4H_4]^{2-}$ complex (depicted in Fig. 17), which has no negative force constants, and all positive electron detachment energies. Indeed, this provides an opportunity for the experimental study of these novel aromatic rings.

Even more, the valence molecular orbitals of $[Al_4H_4]^{2-}$, shown in Fig. 18, correspond to a two-fold aromatic species with two electrons in the π-system and in the tangential system. These two sets of valence molecular orbitals are delocalized on the four aluminums and each of them satisfies the Hückel ($4n + 2$) rule. CMO-NICS values concur with this picture. Nonetheless it is worth mentioning that the overall aromaticity (both NICS(0) = −2.24 ppm and NICS(1) = −6.22 ppm are negative) stems from the occupied π-valence molecular orbitals and that both the tangential and radial valence molecular are antiaromatic, a behavior that parallels[91] that of the aromatic Al_4^{2-} ring.[79]

D_{4h} $[Al_4R_4]^{2-}$ ligands can also be used as aromatic templates for $[M(\kappa^4Al_4H_4)_2]^{2-}$ sandwich like complexes. Fig. 19 depicts the

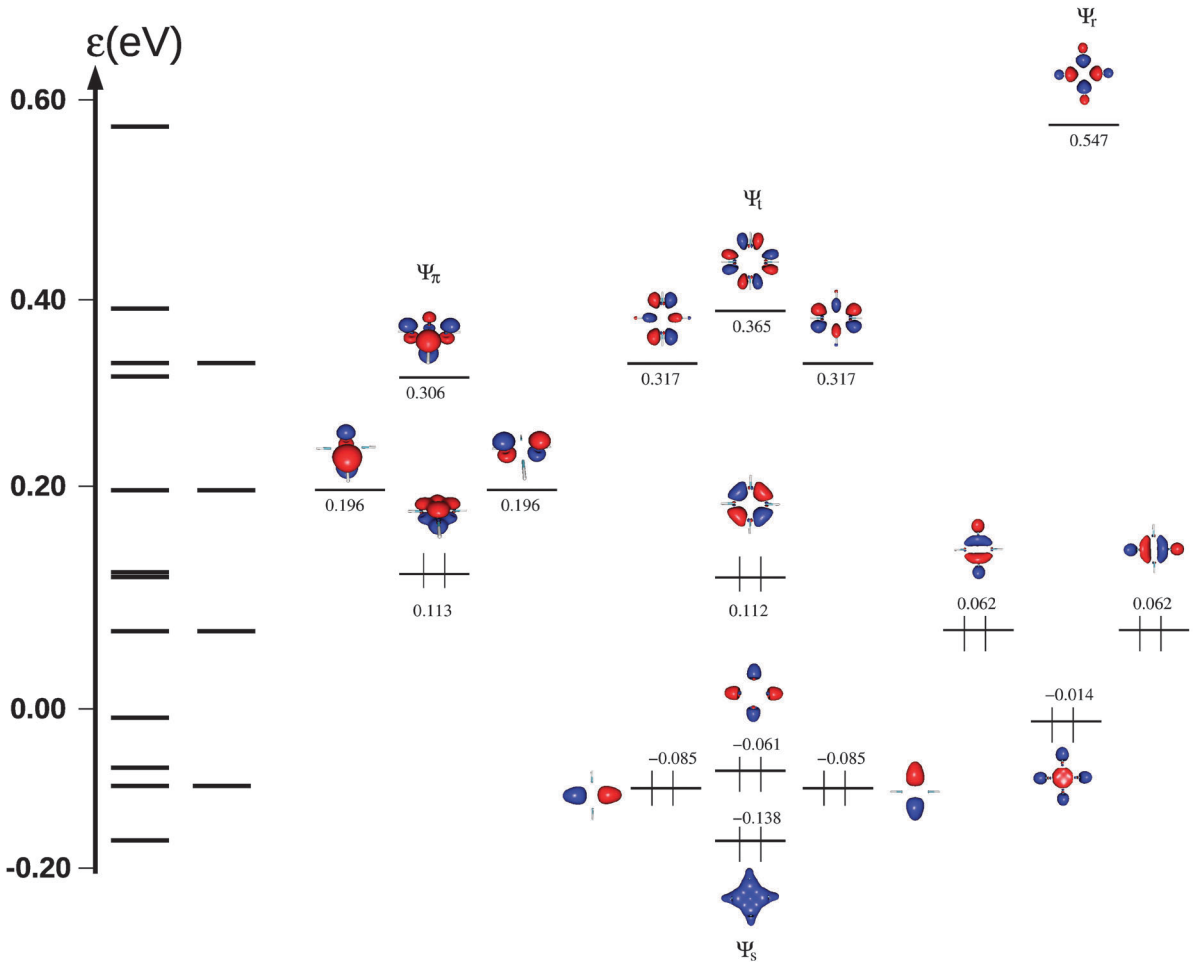

Fig. 18 The valence molecular orbitals of $Al_4H_4^{2-}$.

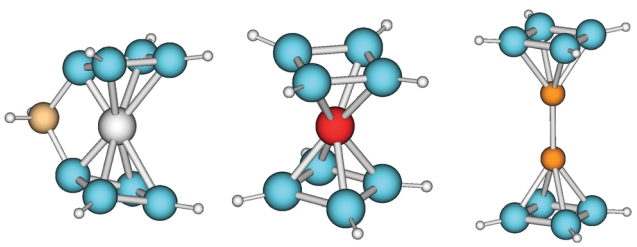

Fig. 19 Optimized structures of *ansa*-$SiH_2[Ti(\kappa^4Al_4H_4)_2]^{2-}$, $[Mn(\kappa^4Al_4H_4)_2]^{2-}$ and $[Mg_2(\kappa^4Al_4H_4)_2]^{2-}$.

stable optimized structures of three representative *model compounds* of such complexes, namely, *ansa*-$SiH_2[Ti(\kappa^4Al_4H_4)_2]^{2-}$, $[Mn(\kappa^4Al_4H_4)_2]^{2-}$ and $[Mg_2(\kappa^4Al_4H_4)_2]^{2-}$. The former has an $^3A_1$ ground state with both unpaired electrons localized on Ti's d-orbitals. The middle structure has an $^6A_1$ ground state with all five unpaired electrons localized on the d^5 orbitals of Mn. Notice that atomic magnetism is not quenched upon complexation. The latter complex has an $^1A_1$ ground state and suggests that the $[Al_4H_4]^{2-}$ ligand can accommodate a central Mg_2^{2+} unit with a single metal–metal bond, which represents an example of a remarkable new class of compounds where reduced s-block elements containing a metal–metal single bond, unsupported by bridging ligands, are sandwiched between two aromatic rings.[133–135] It is worth emphasizing that the bulkiness of the substituents at the aluminium atoms will be a key structural feature for these complexes to have enough stability for its experimental detection.[128]

6 Conclusions

The concepts of aromaticity and antiaromaticity have become very useful to deciphering the electronic structure and assessing the stability of metal clusters. In particular, in this review their great potential has been emphasized to foresee structural patterns of small rings of metal atoms, both, in isolation and incorporated into larger structural units. Advances in a number of key theoretical methods carried out over the last two decades allow to reasonably rationalize the (anti)aromatic nature of the valence electronic structure, as it has been extensively illustrated here for the aromatic Al_4^{2-} cluster. However, much work needs to be done in order to substantiate current discussion on the advantages and reliability of local *versus* non-local indices for (anti)aromaticy studies in metal clusters.

The passivation of metal (anti)aromatic clusters needs to be considered as a means to prevent them from collapsing towards

larger entities, and also to provide protection against the environment. This naturally leads to considering the functionalization of the (anti)aromatic rings and raises new issues related to the interactions of the ligands with the metal ring and the consideration of the effects that those ligands might have on the (anti)aromatic character of the ring. Nonetheless, it opens a vast new playground for cooperation between the experiment and theory that will produce exciting new chemistry in the years ahead.

Acknowledgements

Financial support from Eusko Jaurlaritza (Basque Government) and the Spanish Office for Scientific Research is acknowledged. JMM and JMU thank technical and human support provided by IZO-SGI (SGIker) of UPV/EHU. The work in México was supported by the Moshinsky foundation. This work was supported by the National Science Foundation (CHE-1361413 to A.I.B.). JMU thanks Eusko Jaurlaritza (Basque Government) IT588-13, and the Spanish Office for Scientific Research CTQ2012-38496-C05-01.

References

1 A. Kekulé, *Bull. Soc. Chim. Fr.*, 1865, **3**, 98.
2 A. Kekulé, *Ann. Chem.*, 1872, **162**, 77–124.
3 L. Radom, P. C. Hariharan, J. A. Pople and P. v. R. Schleyer, *J. Am. Chem. Soc.*, 1976, **98**, 10–14.
4 E. Clark, *Polycyclic Hydrocarbons*, Academic Press, New York, 1964.
5 E. Hückel, *Z. Phys.*, 1931, **70**, 204.
6 E. Hückel, *Z. Phys.*, 1931, **72**, 310.
7 E. Hückel, *Z. Phys.*, 1932, **76**, 628.
8 E. Hückel, *Quantentheoretische beiträge zum problem der aromatischen und ungesäigten verbindungen. iii*, Verlag Chem, Berlin, 1938, p. 77.
9 N. C. Baird, *J. Am. Chem. Soc.*, 1972, **94**, 4941–4948.
10 A. Soncini and P. W. Fowler, *Chem. Phys. Lett.*, 2008, **450**, 431–436.
11 F. Feixas, J. Vandenbussche, P. Bultinck, E. Matito and M. Solà, *Phys. Chem. Chem. Phys.*, 2011, **13**, 20690–20703.
12 M. Mandado, A. M. Graña and I. Pérez-Juste, *J. Chem. Phys.*, 2008, **129**, 164114.
13 F. Feixas, E. Matito, J. Poater and M. Solà, in *Applications of Topological Methods in Molecular Chemistry*, ed. R. Chauvin, B. Silvi, C. Lepetit and A. Esmail, Springer, New York, 2015, submitted.
14 M. J. S. Dewar, *Bull. Soc. Chim. Belg.*, 1979, **88**, 957–967.
15 M. J. S. Dewar and M. L. McKee, *Pure Appl. Chem.*, 1980, **52**, 1431–1441.
16 W. Wu, B. Ma, J. I-Chia Wu, P. v. R. Schleyer and Y. Mo, *Chem. – Eur. J.*, 2009, **15**, 9730–9736.
17 Z.-H. Li, D. Moran, K.-N. Fan and P. v. R. Schleyer, *J. Phys. Chem. A*, 2005, **109**, 3711–3716.
18 T. M. Krygowski and B. T. Stepień, *Chem. Rev.*, 2005, **105**, 3482.
19 R. Breslow, *Acc. Chem. Res.*, 1973, **6**, 393–398.
20 A. R. Katritzky, K. Jug and D. C. Oniciu, *Chem. Rev.*, 2001, **101**, 1421.
21 T. M. Krygowski, M. K. Cyrañ, Z. Czarnocki, G. Hälinger and A. R. Katritzky, *Tetrahedron*, 2000, **56**, 1783–1796.
22 A. I. Boldyrev and L.-S. Wang, *Chem. Rev.*, 2005, **105**, 3716.
23 D. L. Thorn and R. Hoffmann, *Nouv. J. Chim.*, 1979, **3**, 39.
24 J. R. Bleeke, *Chem. Rev.*, 2001, **101**, 1205.
25 J. R. Bleeke, *Acc. Chem. Res.*, 2007, **40**, 1035.
26 L. J. Wright, *Dalton Trans.*, 2006, 1821.
27 C. W. Lanford and M. M. Haley, *Angew. Chem., Int. Ed.*, 2006, **45**, 3914–3936.
28 I. Fernández, G. Frenking and G. Merino, *Chem. Soc. Rev.*, 2015, DOI: 10.1039/C5CS00004A.
29 X.-W. Li, W. T. Pennington and G. H. Robinson, *J. Am. Chem. Soc.*, 1995, **117**, 7578.
30 X.-W. Li, Y. Xie, P. R. Schreiner, K. D. Gripper, R. C. Crittendon, C. F. Campana, H. F. Schaefer III and G. H. Robinson, *Organometallics*, 1996, **15**, 3798.
31 G. H. Robinson, *Acc. Chem. Res.*, 1999, **32**, 773.
32 Y. Wang and G. H. Robinson, *Organometallics*, 2007, **26**, 2.
33 Y. Xie, P. R. Schreiner, H. F. Schaefer III, X.-W. Li and G. H. Robinson, *J. Am. Chem. Soc.*, 1996, **118**, 10635.
34 S. C. Critchlow and J. D. Corbett, *Inorg. Chem.*, 1984, **23**, 770.
35 H. J. Breunig, N. Burford and R. Rösler, *Angew. Chem., Int. Ed.*, 2000, **39**, 1521–3773.
36 A. Cisar and J. D. Corbett, *Inorg. Chem.*, 1977, **16**, 2482.
37 R. J. Gillespie and J. Passmore, *Acc. Chem. Res.*, 1971, **4**, 413.
38 I. D. Brown, D. B. Crump and R. J. Gillespie, *Inorg. Chem.*, 1971, **10**, 2319.
39 R. J. Gillespie and G. P. Pez, *Inorg. Chem.*, 1969, **8**, 1229.
40 D. G. Adolphson, J. D. Corbett and D. J. Merryman, *J. Am. Chem. Soc.*, 1976, **98**, 7234.
41 O. J. Scherer, *Angew. Chem., Int. Ed. Engl.*, 1990, **29**, 1104–1122.
42 A. L. Rheingold, M. J. Foley and P. J. Sullivan, *J. Am. Chem. Soc.*, 1982, **104**, 4727–4729.
43 I. Todorov and S. C. Sevov, *Inorg. Chem.*, 1984, **43**, 6490.
44 W. Tiznado, N. Perez-Peralta, R. Islas, A. Toro-Labbe, J. M. Ugalde and G. Merino, *J. Am. Chem. Soc.*, 2009, **131**, 9426.
45 C. S. Wannere, C. Corminboeuf, Z.-X. Wang, M. D. Wodrich, R. B. King and P. v. R. Schleyer, *J. Am. Chem. Soc.*, 2005, **127**, 5701.
46 X. Huang, H. J. Zhai, B. Kiran and L. S. Wang, *Angew. Chem., Int. Ed.*, 2005, **44**, 7215.
47 D. Yu. Zubarev, B. B. Averkiev, H.-J. Zhai, L.-S. Wang and A. I. Boldyrev, *Phys. Chem. Chem. Phys.*, 2008, **10**, 257.
48 B. B. Averkiev and A. I. Boldyrev, *J. Phys. Chem. A*, 2007, **111**, 12864.
49 C. A. Tsipis, *Coord. Chem. Rev.*, 2005, **249**, 2740–2762.
50 D. Y. Zubarev, A. P. Sergeeva and A. I. Boldyrev, in *Chemical Reactivity Theory. A Density Functional View*, ed. P. K. Chattaraj, CRC Press, New York, USA, 2009, pp. 439–452.

51 D. Y. Zubarev and A. I. Boldyrev, in *Computational Inorganic and Bioinorganic Chemistry*, ed. E. I. Solomon, R. A. Scott and B. R. King, Wiley & Sons, Chistester, UK, 2009, pp. 551–562.
52 A. P. Sergeeva, B. B. Averkiev and A. I. Boldyrev, in *Metal-Metal Bonding, volume 136 of Structure and Bonding*, ed. G. Parkin, Springer-Verlag, Berlin, Germany, 2010, pp. 275–306.
53 C. A. Tsipis, in *Metal-Metal Bonding, volume 136 of Structure and Bonding*, ed. G. Parkin, Springer-Verlag, Berlin, Germany, 2010, pp. 217–274.
54 A. P. Sergeeva and A. I. Boldyrev, in *Aromaticity and Metal Clusters*, ed. P. K. Chattaraj, CRC Press, Boca Raton, FL, USA, 2011, ch. 3, pp. 55–68.
55 T. R. Galeev and A. I. Boldyrev, *Annu. Rep. Prog. Chem., Sect. C: Phys. Chem.*, 2011, **107**, 124–147.
56 T. R. Galeev and A. I. Boldyrev, in *Comprehensive Inorganic Chemistry*, ed. J. Reedijk and K. R. Poeppelmeier, Elsevier, Amsterdam, Netherlands, 2013, vol. 9, pp. 245–275.
57 I. A. Popov and A. I. Boldyrev, in *The Chemical Bonding*, ed. G. Frenking and S. Shaik, Wiley VCH, Weinheim, Germany, 2014, pp. 421–444.
58 Z. Chen and R. B. King, *Chem. Rev.*, 2005, **105**, 3613–3642.
59 M. Reiher and A. Hirsch, *Chem. – Eur. J.*, 2003, **9**, 5442.
60 T. M. Krygowski and M. K. Cyrański, *Chem. Rev.*, 2001, **101**, 1385–1420.
61 L. Hanley, J. L. Whitten and S. L. Anderson, *J. Phys. Chem.*, 1988, **92**, 5803–5812. ibid: 1990, 94, 2218.
62 A. Ricca and C. W. Bauschlicher Jr, *Chem. Phys.*, 1996, **208**, 233.
63 J. E. Fowler and J. M. Ugalde, *J. Phys. Chem. A*, 2000, **104**, 397.
64 I. Boustani, *Chem. Phys. Lett.*, 1995, **233**, 273.
65 J.-i. Aihara, *J. Phys. Chem. A*, 2001, **105**, 5486–5489.
66 A. N. Alexandrova, A. I. Boldyrev, H.-J. Zhai and L.-S. Wang, *Coord. Chem. Rev.*, 2006, **250**, 2811.
67 V. Balzani, A. Credi and M. Venturi, *Molecular Devices and Machines: Concepts and Perspectives for the Nanoworld*, Wiley-VCH, Weinheim, Germany, 2nd edn, 2008.
68 T. Heine and G. Merino, *Angew. Chem., Int. Ed.*, 2012, **51**, 10226–10227.
69 G. Martínez-Guajardo, A. P. Sergeeva, A. I. Boldyrev, T. Heine, J. M. Ugalde and G. Merino, *Chem. Commun.*, 2011, **47**, 6242–6244.
70 J. Zhang, A. P. Sergeeva, M. Sparta and A. N. Alexandrova, *Angew. Chem., Int. Ed.*, 2012, **51**, 8512–8515.
71 A. P. Sergeeva, I. A. Popov, Z. A. Piazza, W.-L. Li, C. Romanescu, L.-S. Wang and A. I. Boldyrev, *Acc. Chem. Res.*, 2014, **47**, 1349–1358.
72 D. Y. Zubarev and A. I. Boldyrev, *Phys. Chem. Chem. Phys.*, 2008, **10**, 5207–5217.
73 H.-J. Zhai, A. N. Alexandrova, K. A. Birch, A. I. Boldyrev and L.-S. Wang, *Angew. Chem., Int. Ed.*, 2003, **42**, 6004–6008.
74 T. Heine and G. Merino, *Angew. Chem., Int. Ed.*, 2012, **51**, 4275–4276.
75 T. R. Galeev, C. Romanescu, W.-L. Li, L.-S. Wang and A. I. Boldyrev, *Angew. Chem., Int. Ed.*, 2012, **51**, 2101–2105.
76 C. Romanescu, T. R. Galeev, W.-L. Li, A. I. Boldyrev and L.-S. Wang, *Acc. Chem. Res.*, 2013, **46**, 350–358.
77 P. R. Bunker and P. Jensen, *Fundamentals of Molecular Symmetry*, Series in Chemical Physics, Institue of Physics Publishing, Bristol, UK, 2005.
78 J. M. Mercero, I. Infante and J. M. Ugalde, in *Aromaticity and Metal Clusters*, ed. P. K. Chattaraj, CRC Press, Boca Raton, FL, USA, 2011, ch. 16, pp. 323–337.
79 X. Li, A. E. Kuznetsov, H.-F. Zhang, A. I. Boldyrev and L.-S. Wang, *Science*, 2001, **291**, 859.
80 A. E. Kuznetsov, A. I. Boldyrev, X. Li and L. S. Wang, *J. Am. Chem. Soc.*, 2001, **123**, 8825.
81 D. Y. Zubarev and A. I. Boldyrev, *J. Phys. Chem. A*, 2008, **112**, 7984–7985.
82 C.-G. Zhan, F. Zheng and D. A. Dixon, *J. Am. Chem. Soc.*, 2002, **124**, 14795.
83 R. W. A. Havenith and J. H. van Lenthe, *Chem. Phys. Lett.*, 2004, **385**, 198–201.
84 A. I. Boldyrev and A. E. Kuznetsov, *Inorg. Chem.*, 2002, **41**, 532–537.
85 J. C. Santos, W. Tiznado, R. Contreras and P. Fuentealba, *J. Chem. Phys.*, 2004, **120**, 1670–1673.
86 J. Jusélius, M. Straka and D. Sundholm, *J. Phys. Chem. A*, 2001, **105**, 9939–9944.
87 Y. C. Lin, J. Jusélius, D. Sundholm and J. Gauss, *J. Chem. Phys.*, 2005, **122**, 214308.
88 P. W. Fowler, R. W. A. Havenith and E. Steiner, *Chem. Phys. Lett.*, 2001, **342**, 85–90.
89 P. W. Fowler, R. W. A. Havenith and E. Steiner, *Chem. Phys. Lett.*, 2002, **359**, 530–536.
90 R. W. A. Havenith, P. W. Fowler, E. Steiner, S. Shetty, D. Kanhere and S. Pal, *Phys. Chem. Chem. Phys.*, 2004, **6**, 285–288.
91 Z. Chen, C. Corminbeouf, T. Heine, J. Bohmann and P. v. R. Schleyer, *J. Am. Chem. Soc.*, 2003, **125**, 13930–13931.
92 R. W. A. Havenith and P. W. Fowler, *Phys. Chem. Chem. Phys.*, 2006, **8**, 3383–3386.
93 A. E. Kuznetsov, K. A. Birch, A. I. Boldyrev, X. Li, H. J. Zhai and L. S. Wang, *Science*, 2003, **300**, 622.
94 T. J. Robilotto, J. Bacsa, T. G. Gray and J. P. Sadighi, *Angew. Chem., Int. Ed.*, 2012, **51**, 12077–12080.
95 K. Freitag, C. Gemel, P. Jerabek, M. I. Oppel, R. W. Seidel, G. Frenking, H. Banh, K. Dilchert and R. A. Fischer, *Angew. Chem., Int. Ed.*, 2015, **54**, 4370–4374.
96 X. X. Chi and Y. Liu, *Int. J. Quantum Chem.*, 2007, **107**, 1886–1896.
97 H.-J. Zhai, B. B. Averkiev, D. Y. Zubarev, L.-S. Wang and A. I. Boldyrev, *Angew. Chem., Int. Ed.*, 2007, **46**, 4277.
98 T. Murahashi, R. Inoue, K. Usui and S. Ogoshi, *J. Am. Chem. Soc.*, 2009, **131**, 9888–9889.
99 A. P. Sergeeva and A. I. Boldyrev, *Phys. Chem. Chem. Phys.*, 2010, **12**, 12050–12054.
100 A. C. Tsipis and A. V. Stalikas, *J. Comput. Chem.*, 2011, **32**, 620–638.
101 Z. Badri, S. Pathak, H. Fliegl, P. Rashidi-Ranjbar, R. Bast, R. Marek, C. Foroutan-Nejad and K. Ruud, *J. Chem. Theory Comput.*, 2013, **9**, 4789–4796.

102 C. Foroutan-Nejad, *Theor. Chem. Acc.*, 2015, **134**, 8.
103 A. C. Tsipis and G. N. Gkekasa, *J. Coord. Chem.*, 2014, **67**, 2550–2563.
104 A. C. Tsipis, C. E. Kefalidis and C. A. Tsipis, *J. Am. Chem. Soc.*, 2008, **130**, 9144–9155.
105 C. A. Tsipis, in *Metal-Metal Bonding, volume 136 of Structure and Bonding*, ed. G. Parkin, Spinger, Berlin/Heidelberg, 2010, pp. 217–274.
106 R. Benassi, P. Lazzeretti and F. Taddei, *J. Phys. Chem.*, 1975, **79**, 848–851.
107 T. Heine, C. Corminboeuf and G. Seifert, *Chem. Rev.*, 2005, **105**, 3889–3910.
108 J. Jusélius and D. Sundholm, *Phys. Chem. Chem. Phys.*, 1999, **1**, 3429–3435.
109 H. Fliegl, S. Taubert, O. Lehtonena and D. Sundholm, *Phys. Chem. Chem. Phys.*, 2011, **13**, 20500–20518.
110 Z. Chen, C. S. Wannere, C. Corminboeuf, R. Puchta and P. v. R. Schleyer, *Chem. Rev.*, 2005, **105**, 3842.
111 T. Heine, R. Islas and G. Merino, *J. Comput. Chem.*, 2007, **28**, 302–309.
112 R. Islas, T. Heine and G. Merino, *Acc. Chem. Res.*, 2012, **45**, 215–228.
113 S. Fias, Z. Boisdenghien, T. Stuyver, M. Audiffred, G. Merino, P. Geerlings and F. de Proft, *J. Phys. Chem. A*, 2013, **117**, 3556–3560.
114 A. D. Becke and K. E. Edgecombe, *J. Chem. Phys.*, 1990, **92**, 5397.
115 B. Silvi and A. Savin, *Nature*, 1994, **371**, 683–686.
116 A. Savin, R. Nesper, S. Wengert and T. F. Fässler, *Angew. Chem., Int. Ed. Engl.*, 1997, **36**, 1808–1832.
117 J. Poater, M. Duran, M. Solà and B. Silvi, *Chem. Rev.*, 2005, **105**, 3911–3947.
118 J. M. Mercero and J. M. Ugalde, *J. Am. Chem. Soc.*, 2004, **126**, 3380–3381.
119 J. M. Mercero, E. Formoso, J. M. Matxain, L. A. Eriksson and J. M. Ugalde, *Chem. – Eur. J.*, 2006, **12**, 4495.
120 J. M. Mercero, J. M. Matxain, X. Lopez, D. M. York, A. Largo, L. A. Eriksson and J. M. Ugalde, *Int. J. Mass Spectrom.*, 2005, **240**, 37–99.
121 L.-M. Yang, Y.-H. Ding and C.-C. Sun, *Chem. – Eur. J.*, 2007, **13**, 2546.
122 D.-K. Seo and J. D. Corbett, *Science*, 2001, **291**, 841.
123 R. J. Wright, M. Brynda and P. P. Power, *Angew. Chem., Int. Ed.*, 2006, **45**, 5953.
124 J. M. Mercero, M. Piris, J. M. Matxain, X. Lopez and J. M. Ugalde, *J. Am. Chem. Soc.*, 2004, **131**, 6949–6951.
125 A. Purath, R. Köppe and H. Schnöckel, *Angew. Chem., Int. Ed.*, 1999, **38**, 2926–2928.
126 P. Yang, R. Köppe, T. Duan, J. Hartig, G. Hadiprono, B. Pilawa, I. Keilhauer and H. Schnöckel, *Angew. Chem., Int. Ed.*, 2007, **46**, 3579–3583.
127 C. Dohmeier, H. Schnöckel, U. Schneider, R. Ahlrichs and C. Robl, *Angew. Chem., Int. Ed. Engl.*, 1993, **32**, 1655.
128 H. E. Roesky and S. S. Kumar, *Chem. Commun.*, 2005, 4027–4038.
129 X. Li, A. Grubisic, S. T. Stokes, J. Cordes, G. F. Ganteför, K. H. Bowen, B. Kiran, M. Willis, P. Jena, R. Burger and H. Schnöckel, *Science*, 2007, **315**, 356.
130 A. Grubisic, X. Li, G. F. Ganteföer, K. H. Bowen, B. Kiran, P. Jena, R. Burgert and H. Schnöeckel, *J. Am. Chem. Soc.*, 2007, **129**, 5969–5975.
131 A. J. Welch, *Chem. Commun.*, 2013, **49**, 3615–3616.
132 E. D. Jemmis, M. M. Balakrishnarajan and P. D. Pancharatna, *Chem. Rev.*, 2002, **102**, 93–144.
133 I. Resa, E. Carmona, E. Gutierrez-Puebla and A. Monge, *Science*, 2004, **305**, 1136.
134 S. P. Green, C. Jones and A. Stasch, *Science*, 2007, **318**, 1754.
135 A. Velázquez, I. Fernández, G. Frenking and G. Merino, *Organometallics*, 2007, **26**, 4761.

